Minimizing Trilateration Errors in the Presence of Uncertain Landmark Positions

Alexander Bahr John J. Leonard
Computer Science and Artificial Intelligence Lab, MIT, Cambridge, MA, USA

***Abstract*—Trilateration is a technique for position estimation from range measurements which is often used in robot navigation. Most applications assume that there is no error associated with the landmarks used for trilateration. In cooperative navigation, in which groups of robots use each other as mobile beacons for position estimation, it is imperative to take the uncertainty in the beacon position into account. In this paper, we model the position uncertainty of a landmark using a multivariate Gaussian distribution and show how the uncertain landmark position translates to an uncertainty in the trilaterated position. We provide insights into how the optimal trilateration point for a fixed geometry of landmarks depends on the distribution of the position error. This provides a metric for guiding the motion of a robot to maintain favorable trilateration geometries when navigating relative to other robots whose positions are imprecisely known.**

***Index Terms*—Trilateration, Cooperative Navigation, Mobile Robots, Uncertain Landmarks**

I. Motivation

Trilateration is a technique where the unknown position of an object is determined through *range* measurements to landmarks at known locations, while triangulation uses *angle* measurements to landmarks to obtain a position estimate. Both techniques have been in use for many years, mostly for geodesy and maritime navigation. Even today's most sophisticated navigation systems rely on their basic principles. For example GPS-receivers estimate their positions through trilateration to satellites at known positions and aircraft use radio beacons for triangulation.

Mobile robots use a variety of sensors to obtain ranges or angles (or both) to landmarks and then use trilateration and triangulation to obtain a position estimate. Some sensors, such as cameras, are able to provide accurate angle measurements at high update rates while others, such as sonar sensors, provide range measurements. An increasing number of sensors, such as stereo cameras or 2D-laser range finders are able to provide both, range and angle. The size of a robot and the environment in which it operates often constrain the type of sensors used. Underwater vehicles which can usually not rely on optical instruments (cameras and laser range finders) are usually limited to range information provided by time-of-flight measurements (figure 1). This paper will focus on trilateration.

All geodesy applications and most early work in mobile robotics used easily distinguishable features in the environment or fixed beacons as landmarks for triangulation. The positions of these landmarks or beacons was assumed to be error free. It was also significantly smaller than the error associated with the range or angle measurement and could therefore be ignored. Both assumptions do not hold once groups of robots are introduced which use each other as landmarks. Now a robot uses a landmark whose position has an uncertainty associated with it which is too significant to be ignored. This uncertainty is now known, as the "landmark"-robot can use an error model which uses the distance traveled and knowledge of the proprioceptive sensor noise to compute a probability distribution of its position and can broadcast it to other robots which can then use this information. Knowing the uncertainty associated with the position of our landmarks, we can now quantify how it affects the uncertainty of the position derived from these landmarks through trilateration.

Fig. 1. An Autonomous Underwater Vehicle (AUV), here surfaced (foreground) uses and Autonomous Surface Craft (ASC) (background) as a navigation aid. The GPS-derived position of the ASC is obtained by the submerged AUV through an acoustic modem. Using time-stamped messages and globally synchronized clocks on all vehicles the AUV is also able to determine its range to the ASC through time-of-flight measurements.

In this paper we will first introduce trilateration based on two landmarks and then derive how uncertainty in the landmark position, modeled through a bivariate Gaussian distribution, affects the uncertainty of the obtained position. We then show how the distribution of the landmark's uncertainty not

only affects the magnitude of trilaterated position uncertainty, but also the robot's position with respect to the landmarks from which trilateration would lead to minimum position uncertainty. Being able to determine the position which minimizes the trilateration error is important in a scenario where some robots in a group are dedicated navigation beacons and therefore have to adapt their position accordingly.

II. Related Work

Trilateration has numerous applications, and has been the subject of extensive research outside of the robotics community. In particular, GPS navigation relies on trilateration to satellites at known positions, and hence there is a large body of work that addresses the uncertainty of trilateration fixes. The metric most frequently employed is the Geometric Dilution of Precision (GDOP), a single dimensionless number which captures the influence of the geometry on the error of the position estimate. Examples of work that investigates error metrics for GPS trilateration includes Chaffee and Abel [1] and McKay and Pachter [2]. This literature typically assumes precise knowledge of the positions of satellites, and hence the impact of the beacon position error is not analyzed.

Early work in multi-robot localization, which used the concept of "portable landmarks", where a stationary group of robots would serve as landmarks to a moving group of landmarks, did not take the trilateration and triangulation-error into account [3]. Later, more dynamic scenarios were investigated where all robots tried to improve their position estimate through range or angle-measurements to other robots [4]. Here the uncertainty estimate of the landmarks (other robots) was used implicitly during the position estimate, but no attempt was made to explicitly analyze its magnitude and its dependence on the geometry.

Simultaneous Localization and Mapping (SLAM) generalizes localization to include building a map of the environment. In feature-based SLAM, the environment is typically represented in terms of discrete landmarks, and hence in such a formulation uncertainty in the landmark location is incorporated explicitly. Feature-based SLAM from range-only measurements has been addressed by several authors, including Djugash *et al.* [5], who developed SLAM algorithms for range-only measurements using custom sensor nodes, and Wijk and Christensen [6], who performed SLAM via trilateration of range measurements from ultrasonic sensors. In a SLAM formulation, the position estimate for the vehicle implicitly accounts for the (correlated) uncertainty in the position estimates of the landmarks. To our knowledge, however, the range-only SLAM literature has not addressed the topic of the effect of beacon position uncertainty on the solution geometry, which is the topic of this paper.

Trilateration is a central component of methods to calibrate the positions of networks of sensors with range-only measurement capabilities. Moore [7] presents an algorithm which selects landmarks for trilateration such that the geometry ensures that the solution is unique in the presence of measurement noise.

Work that specifically investigates the error of trilateration- (or triangulation-) based localization techniques is fairly sparse when compared to their widespread use. Kelly [8] provides a good and intuitive insight into the relation between robot/landmark-geometry and the resulting position accuracy, but he does not take the uncertainty of the landmarks into account. Easton and Cameron [9] explicitly assume noisy landmarks for triangulation-based algorithms, but their method does not consider the effects of strongly skewed error distributions (as shown in figure 2) and their effect on the optimal triangulation geometry. As a result, the uncertainty of his triangulated position is affected by the sensor noise, but the point where triangulation leads to the smallest possible error for given landmark uncertainties does not vary.

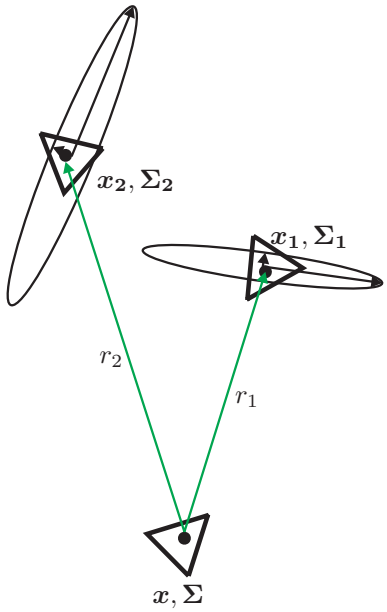

Fig. 2. Robot triangulating its position $\boldsymbol{x}$ using range measurements r_1 and r_2 to robots at known locations $\boldsymbol{x_1}$ and $\boldsymbol{x_2}$.

III. Trilateration

The trilateration problem for ranges to two landmarks, shown in figure 2, can be expressed in closed form and is posed as follows. A robot tries to estimate its position $\boldsymbol{x} = [x, y]^T$ using range measurements r_1 and r_2 to landmarks l_1 and l_2 at known positions $\boldsymbol{x_1} = [x_1, y_1]^T$ and $\boldsymbol{x_2} = [x_2, y_2]^T$.

The intersection of the two range circles

$$\boldsymbol{X} = \mathcal{F}(\boldsymbol{x}_1, \boldsymbol{x}_2, r_1, r_2) \tag{1}$$

leads to zero, one or two solutions

$$\boldsymbol{X} = \emptyset \qquad \text{or} \qquad \boldsymbol{X} = \boldsymbol{x1} \qquad \text{or} \qquad \boldsymbol{X} = \begin{pmatrix} \boldsymbol{x1} \\ \boldsymbol{x2} \end{pmatrix}$$

The equations representing $\mathcal{F}$ as well as the Jacobian (3) can be found at

people.csail.mit.edu/∼abahr/publications/publications_ECMR2007_detail.htm

For the remaining discussion we assume that we obtained one or two solutions. In the case of two solutions, further information is necessary to break the ambiguity. This information can be a previous estimate of the robot's position or a position tuple obtained using range measurements to different landmarks. An algorithm for the computation of

the position based on a series of range-measurement pairs is described in [10]. We further assume that the landmarks can be uniquely identified. This is a valid assumption in the case where dedicated beacons or other robots are used for trilateration which usually provide unique IDs.

IV. Error Propagation

To model the error associated with the two landmarks, we assume bivariate Gaussian distributions with mean $\boldsymbol{x_1}$ and $\boldsymbol{x_2}$ and associated covariance matrices $\boldsymbol{\Sigma_1}$ and $\boldsymbol{\Sigma_2}$.

$$\boldsymbol{\Sigma_n} = \begin{bmatrix} {\sigma_{xxn}}^2 & {\sigma_{xyn}}^2 \\ {\sigma_{yxn}}^2 & {\sigma_{yyn}}^2 \end{bmatrix},\ n = [1, 2]$$

Graphically the error is represented by the error ellipse which is typically the 3σ bound which contains 95% of all realizations for $\boldsymbol{x_1}$ and $\boldsymbol{x_2}$. σ_1 and σ_2 are the semi-minor and semi-major axis of the error ellipse which are the eigenvalues of Σ_n.

The Gaussian assumption is not always a valid model for the error distribution of a landmark, but it can be used to provide a conservative estimate if the true error distribution is only similar to a Gaussian. Furthermore many feature-based maps describe the error associated with the features as a bivariate Gaussian and in the case of a cooperative navigation scenario, where robots use each other as landmarks, the landmark positions $\boldsymbol{x_1}$ and $\boldsymbol{x_2}$ are the estimated positions of the cooperating robots. The robots often use a Kalman-filter based navigation engine for dead-reckoning and sensor fusion which also keeps track of the uncertainty associated with the position estimate through a covariance matrix [11]. The positions $\boldsymbol{x_1}$ and $\boldsymbol{x_2}$ and the associated uncertainties $\boldsymbol{\Sigma_1}$ and $\boldsymbol{\Sigma_2}$ are then retrieved from the local Kalman filter of the cooperating robots and transmitted to the trilaterating robot.

The error associated with the computed position of the trilaterating robot is represented by the covariance matrix

$$\boldsymbol{\Sigma} = \begin{bmatrix} {\sigma_{xx}}^2 & {\sigma_{xy}}^2 \\ {\sigma_{yx}}^2 & {\sigma_{yy}}^2 \end{bmatrix}$$

which is given by

$$\boldsymbol{\Sigma} = \boldsymbol{J}\boldsymbol{G}\boldsymbol{J}^T \tag{2}$$

where $\boldsymbol{J}$ is the Jacobian of the intersection function $\mathcal{F}(\boldsymbol{x}_1, \boldsymbol{x}_2, r_1, r_2)$ given by

$$\boldsymbol{J} = \begin{bmatrix} \frac{\partial x}{\partial x_1} & \frac{\partial x}{\partial y_1} & \frac{\partial x}{\partial x_2} & \frac{\partial x}{\partial y_2} & \frac{\partial x}{\partial r_1} & \frac{\partial x}{\partial r_2} \\ \frac{\partial y}{\partial x_1} & \frac{\partial y}{\partial y_1} & \frac{\partial y}{\partial x_2} & \frac{\partial y}{\partial y_2} & \frac{\partial y}{\partial r_1} & \frac{\partial y}{\partial r_2} \end{bmatrix} \tag{3}$$

and

$$\boldsymbol{G} = \begin{bmatrix} {\sigma_{xx1}}^2 & {\sigma_{xy1}}^2 & 0 & 0 & 0 & 0 \\ {\sigma_{yx1}}^2 & {\sigma_{yy1}}^2 & 0 & 0 & 0 & 0 \\ 0 & 0 & {\sigma_{xx2}}^2 & {\sigma_{xy2}}^2 & 0 & 0 \\ 0 & 0 & {\sigma_{yx2}}^2 & {\sigma_{yy2}}^2 & 0 & 0 \\ 0 & 0 & 0 & 0 & {\sigma_{r1}}^2 & 0 \\ 0 & 0 & 0 & 0 & 0 & {\sigma_{r2}}^2 \end{bmatrix}$$

The above structure of G assumes that the uncertainties associated with the positions $\boldsymbol{x_1}$ and $\boldsymbol{x_2}$ are independent, which leads to zeros in the off-diagonal blocks. This can be assumed if the landmarks are features on an a-priori map, but one must be careful in the case of cooperating robots. The following example illustrates the difficulties that arise in such a scenario. A robot $\boldsymbol{V}_1$ uses two other robots $\boldsymbol{V}_2$ and $\boldsymbol{V}_3$ to trilaterate its position and uses the obtained position to fully reset its navigation engine or as an update step in the Kalman filter. As a result the position estimate of $\boldsymbol{V}_1$ is now coupled to the position estimate of $\boldsymbol{V}_2$ and $\boldsymbol{V}_3$. If at a later time robot $\boldsymbol{V}_3$ uses robots $\boldsymbol{V}_2$ and $\boldsymbol{V}_1$ to trilaterate its position, the off-diagonal blocks of G are non-zero as the position estimates $\boldsymbol{x_1}$ and $\boldsymbol{x_3}$ are now coupled. Extra steps must now be taken to obtain the coupling terms and properly populate G. Another possibility is the use of an estimation algorithm, such as *Covariance Intersection* [12] which can fuse information consistently without using the correlation which then leads to more conservative but uncoupled position estimates.

A. Metrics

Two metrics are widely used to describe the error ellipse of a bivariate Gaussian distribution with a single parameter [9]. The area A of the 3σ-error ellipse which is related to the covariance matrix Σ by $A = \pi * \sqrt{det(\Sigma)}$ and the ratio of the semi-minor to the semi-major axis of the error ellipse $\rho = \frac{\sigma_1}{\sigma_2}, (\sigma_1 < \sigma_2)$. While the area A is a useful parameter for $\rho \approx 1$, it does not capture the error for elongated ellipses well. ρ describes the elongation of the ellipse well, but does not provide any information about its overall size.

As both metrics are not adequate to describe the error ellipse we propose to use a variation of the Circular Error Probability (CEP). Most of the literature defines the CEP as the probability $P(R)$ for which a single realization of a mean-free, bivariate Gaussian distribution $N(0, \Sigma)$ is within a circle with radius R around the origin [13]. A variation which defines the CEP as the radius $R(P)$ of the circle which contains half the realizations (for $P = 0.5$) of $N(0, \Sigma)$ is described by Torrieri [14]. There is no closed form solution for $P(R)$ or $R(P)$, but Shnidman provides an efficient algorithm to compute $R(P)$ [15]. Shnidman's algorithm can also be generalized for $P \neq 0.5$, but as $R(P = 0.5)$ provides a parameter with an intuitive understanding of an "average error", all further references to R are $R(P = 0.5)$. For $\rho << 1$ Shnidman's algorithm can run into underflow problems, but as in this case the bivariate is approaching a one-dimensional Gaussian with variance σ_2, we can compute R using the inverse error function.

$$R = \sqrt{2} * \sigma_2 * \text{erf}^{-1}(P) \tag{4}$$

A function to evaluate the inverse error function is provided in MATLAB or is described in [16].

B. Geometry

As the error of the position estimate obtained through trilateration depends strongly on the relative position of the robot to the landmarks, we want to pick an optimal position before trilaterating. A position change which might be necessary to obtain the trilateration result with the least amount of

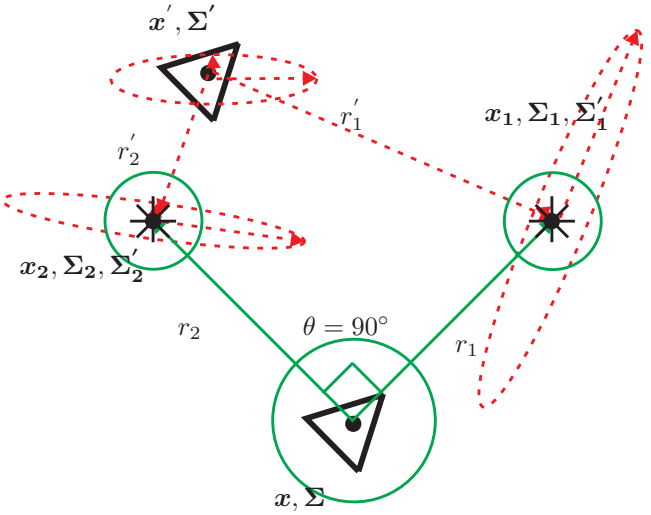

Fig. 3. Optimal trilateration positions for different error distributions. green, solid: $\sigma_1 = \sigma_2$ and $\Sigma_1 = \Sigma_2$. red, dashed: $\sigma_1 << \sigma_2$ and $\Sigma_1 \neq \Sigma_2$

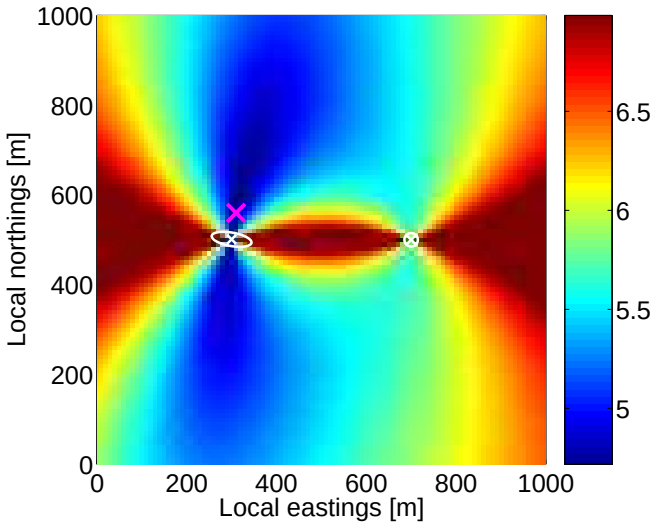

Fig. 4. Error associated with trilateration represented by $\log(A)$ for a given set of two landmarks and their associated position uncertainty (white). The position from which a trilateration would lead to a position estimated with the smallest associated uncertainty is marked by a cross (magenta).

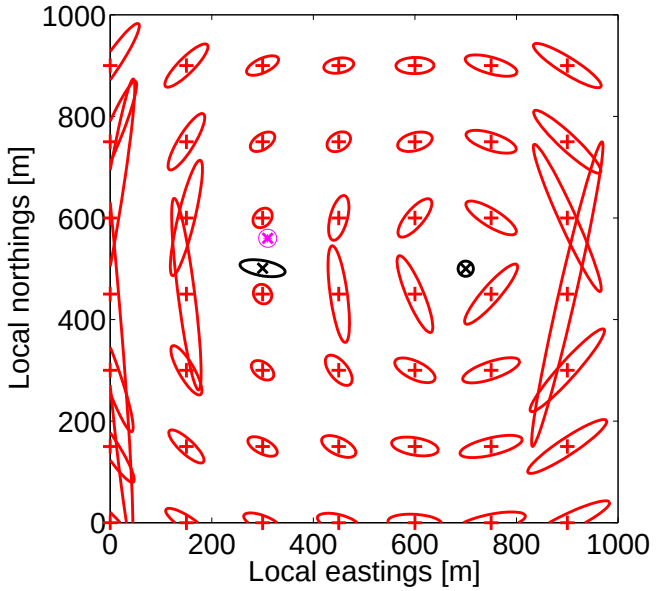

Fig. 5. Same setup as in figure 4 (black: landmarks; magenta: optimal trilateration position). Here the uncertainties associated with trilateration are plotted for selected grid points (red). Note the large error associated with near collinear settings.

associated uncertainty can be done actively by moving the robot to that point or passively by selecting the appropriate pair of landmarks, in case more than two are available, such that the optimal trilateration point moves closer to the robot's. In the case where $\sigma_1 = \sigma_2$ the optimal position of the robot is in the corner of a rectangular triangle with the landmarks in the two other corners [8], but in case where $\sigma_1 << \sigma_2$ for Σ_1 or Σ_2 the optimal position strongly depends on the shape and orientation (see figure 3) of the error ellipses.

V. Analysis

To analyze the effect of various uncertainty distributions of the landmarks, we choose the following setup for figures 4-8: We set up a 1000 by 1000 point grid where landmark l_1 is fixed at $\boldsymbol{x_1} = [300, 500]^T$ and landmark l_2 at $\boldsymbol{x_2} = [700, 500]^T$. The robot is placed at all grid points $\boldsymbol{x}(i, j)$ in 10 unit-increments. We then compute the ranges r_1 and r_2 to l_1 and l_2. Using these ranges we trilaterate our position using (1) and obtain two positions $\boldsymbol{x1}$ and $\boldsymbol{x2}$, one of which is $\boldsymbol{x}(i, j)$ and the other one is its mirror solution $\boldsymbol{x}'(i, \|500 - j\|)$. As we assume that we have resolved the ambiguity we can select $\boldsymbol{x1}$ or $\boldsymbol{x2}$ based on which one is equal to $\boldsymbol{x}(i, j)$. Knowing which one of the two is the correct solution, we can select the appropriate Jacobian J and can then compute Σ using (2). The variance associated with the range measurements r_1 and r_2 is fixed to $\sigma_{r1}^2 = \sigma_{r2}^2 = 3^2$ for all cases, but the variances Σ_1 and Σ_2 change.

First, we select a circular uncertainty distribution for l_2 with $\sigma_{xx2}^2 = \sigma_{yy2}^2 = 5^2$. The uncertainty Σ_1 for l_1 is an ellipse with $\sigma_1^2 = 5^2$ and $\sigma_2^2 = 15^2$ which is rotated by $85°$. Figure 4 shows the uncertainty associated with the trilaterated position for each grid point. Note how despite the symmetric setup of the landmarks, the distribution of the uncertainty is not symmetric. The results for the collinear case where $\boldsymbol{x} = [x, 500]^T$ were clipped as the uncertainty is infinite.

Figure 5 shows the same setup. This time uncertainty for all grid points was omitted and the covariance ellipses were plotted for a selected number of grid points.

Figures 6 and 7 show the evolution of the optimal trilateration point as an ellipse for Σ_1 with $\sigma_1^2 = 3^2$ and $\sigma_2^2 = 15^2$ is rotated counter-clockwise by $180°$ from its original position (red: $0°$; green: $90°$). Σ_2 remained unchanged and is asymmetric in figure 6 with $\sigma_{xx2}^2 = 3^2$ and $\sigma_{yy2}^2 = 7^2$ and symmetric in figure 7 with $\sigma_{xx2}^2 = \sigma_{yy2}^2 = 5^2$.

For figure 8 we choose circular distributions for Σ_1 and Σ_2. While Σ_2 remained constant the elements of Σ_1 changed from $\sigma_{xx1}^2 = \sigma_{yy1}^2 = 5^2$ to $\sigma_{xx1}^2 = \sigma_{yy1}^2 = 15^2$. This affected the magnitude of the uncertainty at every grid point, but did not change the position of the optimal trilateration point which forms a rectangular triangle with both landmarks opposite to

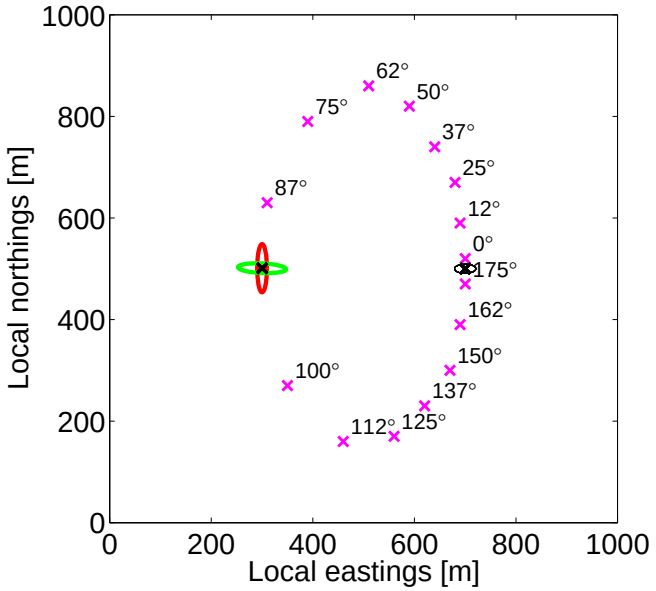

Fig. 6. Trajectory of the optimal trilateration point as the error ellipse of landmark l_1 is rotated by $180°$. (red: $0°/180°$-position; green: $90°$-position). The crosses indicate the optimal trilateration point for selected angles. The error distribution for landmark l_2 is *elliptic*.

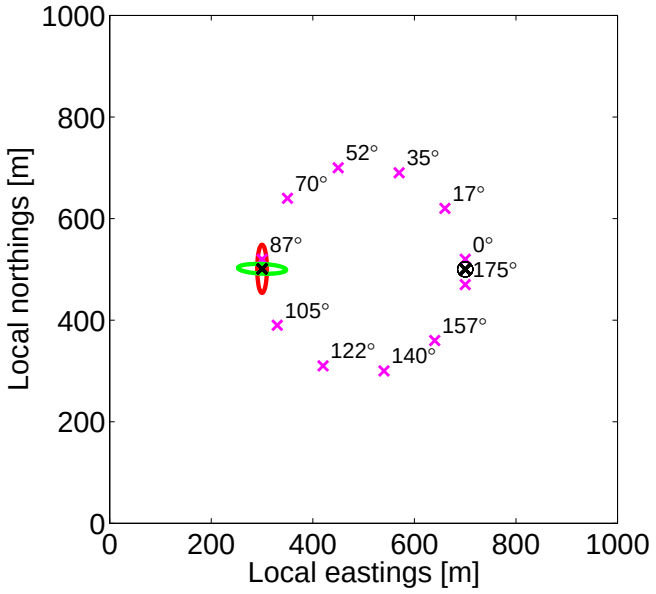

Fig. 7. Trajectory of the optimal trilateration point as the error ellipse of landmark l_1 is rotated by $180°$. (red: $0°/180°$-position; green: $90°$-position). The crosses indicate the optimal trilateration point for selected angles. The error distribution for landmark l_2 is *circular*.

the perpendicular angle, just as in the case where the position uncertainty of the landmarks is assumed to be 0.

Note that throughout the previous discussion the notion of an optimal trilateration point also has an important meaning for *tracking* applications which is the inverse to trilateration or triangulation depending on what type of information (range or angle) is used. If the two robots in figure 3 at $\boldsymbol{x}_1$ and $\boldsymbol{x}_2$ with corresponding position uncertainties Σ_1 and Σ_2 were to track the "target"-robot at $\boldsymbol{x}$ using nothing but the ranges r_1 and r_2 while maintaining a fixed distance $\overline{\boldsymbol{x}_1, \boldsymbol{x}_2}$, the positions $\boldsymbol{x}_1$

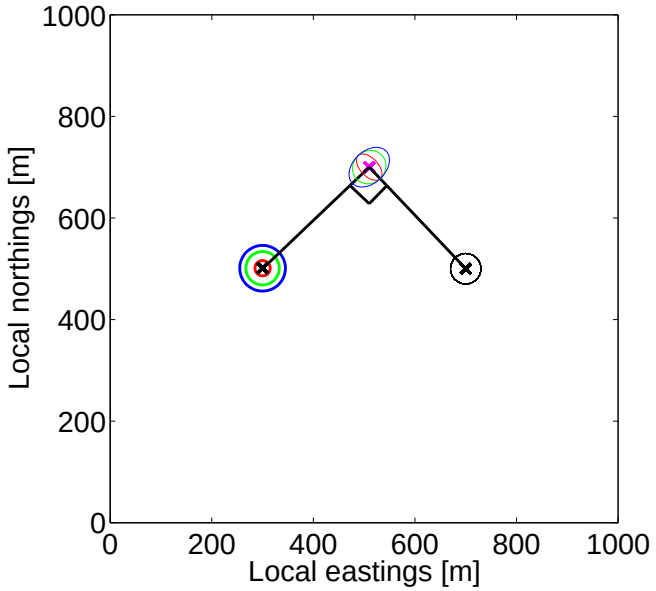

Fig. 8. Optimal trilateration point (magenta) for a *circular* error distribution for landmark l_1 and l_2. The size of the covariance ellipse for l_1 grows from $\sigma^2_{xx1} = \sigma^2_{yy1} = 5^2$ to $\sigma^2_{xx1} = \sigma^2_{yy1} = 15^2$ (red, green and blue circle around l_1). Note that while the uncertainty of the position estimate does change, the optimal trilateration position does not. It remains at the corner of a rectangular triangle as shown in figure 3.

and $\boldsymbol{x}_2$ would be the optimal tracking positions for a target robot at $\boldsymbol{x}$.

VI. Application

An example for cooperative navigation is the Moving Long Baseline (MLBL)-concept presented in [17] where a dedicated group of Autonomous Underwater Vehicles (AUVs) called Communication And Navigation Aids (CNAs) has very sophisticated navigation sensors and broadcasts its position over an acoustic modem. As all vehicles have access to globally synchronized clocks, the time-stamped messages sent over the acoustic modem can also be used to obtain range information to the broadcasting vehicle through one-way travel times. This way a large group of AUVs with poor navigation sensors which is within communication range of the CNAs can maintain high navigation accuracy. The modem we use has been developed by the Acoustic Communications Group at the Woods Hole Oceanographic Institution (WHOI) and is described in [18]. As an intermediate step we used Autonomous Surface Crafts (ASCs) — kayaks outfitted with propulsion, a PC, GPS (Garmin GPS 18 5Hz) and an acoustic modem — as CNAs. An AUV was then set up to run a U-shaped trackline (figure 9) while the following ASCs broadcasted their GPS-derived position over the acoustic modem (picture 1). As only one range/position pair is obtained every 10 seconds, a combination of dead-reckoning and trilateration described in [10] must be used to obtain a position estimate. Figure 9 shows the navigation obtained by post-processing the dead-reckoning information (blue). In the absence of GPS underwater this post-processing result taking the GPS information before the dive and after surfacing into account is considered "ground-truth" here. Throughout the run the AUV received

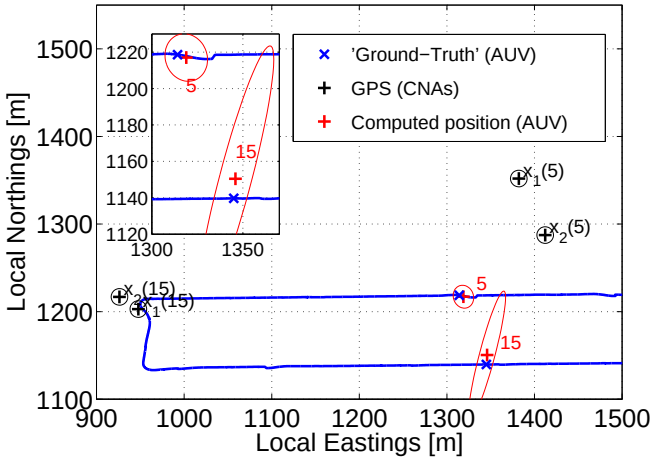

Fig. 9. MLBL experiment with two ASCs and one AUV showing "ground-truth" and trilaterated positions at $t = 5$ (favorable geometry) and $t = 15$ (unfavorable geometry). Blue: trackline of the AUV using the post-processed dead-reckoning results. Red: trilaterated positions of the AUV with associated uncertainty. Black: positions of the CNAs at the time of trilateration. Detail: trilaterated solutions.

enough range/position pairs to trilaterate 15 position estimates together with their associated uncertainty. Two of them, $\boldsymbol{x}(5)$ and $\boldsymbol{x}(15)$ are shown together with the associated uncertainty ellipse (red) and the position of the CNAs at that time (black). The position uncertainty of the CNAs was indicated by the GPS receiver to be $\sigma^2_{xx} = \sigma^2_{yy} = 3^2$ for both vehicles and did not change as the kayaks had a clear view of the sky through the entire run. The variance for range measurements was set to $\sigma^2_{r1} = \sigma^2_{r2} = 3^2$. The position $\boldsymbol{x}(5)$, which was obtained from the CNAs at $\boldsymbol{x}_1(5)$ and $\boldsymbol{x}_2(5)$ under a much more favorable geometry than $\boldsymbol{x}(15)$ using the almost collinear geometry created by the CNAs at $\boldsymbol{x}_1(15)$ and $\boldsymbol{x}_2(15)$ leads to a much smaller position uncertainty for $\boldsymbol{x}(5)$ than for $\boldsymbol{x}(15)$ as indicated by the covariance ellipse. The detail in the upper left corner shows a magnification of the trilaterated solutions (red "x") together with the "ground-truth" at the same point in time (blue "x") where the trilaterated position $\boldsymbol{x}(5)$ is closer to the "ground-truth" than $\boldsymbol{x}(15)$.

VII. Conclusion and Future Work

We derived a framework which allows us to compute the uncertainty associated with a trilaterated position for the case of landmarks with uncertain positions. We then showed how the orientation and size of the error distribution associated with the landmarks significantly affects the trilateration error and how subsequently the point for optimal trilateration changes.

This analysis will be used in future work to develop an algorithm which can control the motion of the AUVs to optimize the trilateration geometry in real-time. The trajectories presented here provide the insights to facilitate this development. Being able to efficiently compute the optimal trilateration point will enable us to use this point as a goal for path planning strategies geared to optimize cooperative navigation. We are also looking into the pairwise computation of trilateration uncertainties in order to select an optimal set of $n, (n > 2)$ landmarks from a set of $m, (m \geq n)$ landmarks which will lead to an optimal trilateration result for a least-square-based algorithm.

Acknowledgments

The authors wish to thank the people who helped during the experiment at *NSWC* Panama City, FL in December 2006 where the experimental data were gathered, namely Joseph Curcio, Iuliu Vasilescu, Jerome Vaganay, Matt Lockhardt and Joseph Daverin. This work was supported in part by ONR grants N00014-02-C-0210, N00014-97-1-0202 and N00014-05-G-0106, and by the MIT Sea Grant College Program under grant NA86RG0074 (project RD-24).

References

[1] J. Chaffee and J. Abel, "GDOP and the cramer-rao bound," in *Proc. IEEE Symposium on Position Location and Navigation*, Las Vegas, NV, USA, 1994.

[2] J. B. McKay and M. Pachter, "Geometry optimization for GPS navigation," in *Proc. IEEE Conference on Decision and Control*, San Diego, CA, USA, 1997.

[3] R. Kurazume, S. Hirose, and S. Nagata, "Study on cooperative positioning system," in *Proc. IEEE Int. Conf. Robotics and Automation*, Minneapolis, MN, USA, 1996, pp. 1421–1426.

[4] S. I. Roumeliotis and I. Rekleitis, "Analysis of multirobot localization uncertainty propagation," in *Proc. IEEE Int. Workshop on Intelligent Robots and Systems*, Las Vegas, NV, USA, 2003, pp. 1763–1770.

[5] J. Djugash, G. Kantor, S. Singh, and W. Zhang, "Range-only slam for robots operating cooperatively with sensor networks," in *Proc. International Conference on Robotics and Automation*, may 2006.

[6] O. Wijk and H. Christensen, "Triangulation based fusion of sonar data with application in robot pose tracking," *IEEE Trans. Robotics and Automation*, vol. 16, no. 6, pp. 740–752, December 2000.

[7] D. Moore, J. Leonard, D. Rus, and S. Teller, "Robust distributed network localization with noisy range measurements," in *SenSys '04: Proceedings of the 2nd international conference on Embedded networked sensor systems*. New York, NY, USA: ACM Press, 2004, pp. 50–61.

[8] A. Kelly, "Precision dilution in triangulation based mobile robot position estimation," in *Proc. of the 8th Int. Conf. on Intelligent Autonomous Systems*, Amsterdam, Netherlands, 2003, p. submitted for publication.

[9] A. Easton and S. Cameron, "A gaussian error model for triangulation-based pose estimation using noisy landmarks," in *Proc. IEEE International Conference on Robotics, Automation and Mechatronics*, Bangkok, Thailand, 2006, p. submitted for publication.

[10] A. Bahr and J. Leonard, "Cooperative localization for autonomous underwater vehicles," in *Proc. 10th International Symposium on Experimental Robotics (ISER)*, Rio de Janeiro, Brazil, 2006.

[11] J. J. Leonard and H. F. Durrant-Whyte, "Mobile robot localization by tracking geometric beacons," *IEEE Trans. Robotics and Automation*, vol. 7, no. 3, pp. 376–382, June 1991.

[12] S. J. Julier and J. K. Uhlmann, "A non-divergent estimation algorithm in the presence of unknown correlations," in *Proc. American Control Conference*, Albuquerque, New Mexico, USA, 1997.

[13] J. Gillis, "Computation of the circular error probability integral," *IEEE Trans. Aerospace and Electronic Systems*, vol. 27, no. 6, pp. 906–910, 1991.

[14] D. Torrieri, "Statistical theory of passive location systems," *IEEE Trans. Aerospace and Electronic Systems*, vol. 20, no. 2, pp. 183–197, 1984.

[15] D. Shnidman, "Efficient computation of the circular error probability (cep) integral," *IEEE J. Robotics and Automation*, vol. 40, no. 8, pp. 1472–1474, 1995.

[16] S. Winitzki, "A handy approximation for the error function and its inverse," lecture note, 2006.

[17] J. Vaganay, J. Leonard, J. Curcio, and J. Wilcox, "Experimental validation of the moving long base-line navigation concept," in *Proc. IEEE conference on Autonomous Underwater Vehicles*, 2004, pp. 59–65.

[18] L. Freitag, M. Grund, S. Singh, J. Partan, and K. Ball, "The WHOI micro-modem: An acoustic communications and navigation system for multiple platforms," in *IEEE OCEANS 2005*, Washington, DC, USA, 2005.